

# Journal of Materials Chemistry B

Materials for biology and medicine

Accepted Manuscript

This article can be cited before page numbers have been issued, to do this please use: J. Lu, Z. Li, X. Zheng, J. Tan, Z. Ji, Z. Sun and J. You, *J. Mater. Chem. B*, 2020, DOI: 10.1039/D0TB01970D.



This is an Accepted Manuscript, which has been through the Royal Society of Chemistry peer review process and has been accepted for publication.

Accepted Manuscripts are published online shortly after acceptance, before technical editing, formatting and proof reading. Using this free service, authors can make their results available to the community, in citable form, before we publish the edited article. We will replace this Accepted Manuscript with the edited and formatted Advance Article as soon as it is available.

You can find more information about Accepted Manuscripts in the [Information for Authors](#).

Please note that technical editing may introduce minor changes to the text and/or graphics, which may alter content. The journal's standard [Terms & Conditions](#) and the [Ethical guidelines](#) still apply. In no event shall the Royal Society of Chemistry be held responsible for any errors or omissions in this Accepted Manuscript or any consequences arising from the use of any information it contains.

# A Rapid Response Near-infrared Ratiometric Fluorescent Probe Enabled In Real-Time Peroxynitrite Tracking for Pathological Diagnosing and Therapeutic Assessment in Rheumatoid Arthritis Model

Received 00th January 20xx,  
Accepted 00th January 20xx

DOI: 10.1039/x0xx00000x

Jiao Lu<sup>†</sup>, Zan Li<sup>\*†</sup>, Xinrui Zheng<sup>†</sup>, Jiangkun Tan<sup>†</sup>, Zhongyin Ji<sup>†</sup>, Zhiwei Sun<sup>†</sup>, Jinmao You<sup>\*†</sup>

Peroxynitrite (ONOO<sup>-</sup>) is a potent bio-oxidant involved in many physiological and pathological processes, however, most of the pathological effects associated with ONOO<sup>-</sup> *in vivo* are still ambiguous. Herein, we design and synthesize two near-infrared ratiometric fluorescent probes **Ratio-A** and **Ratio-B** for ONOO<sup>-</sup> detection and biological evaluation. The recognition unit diene in the probes can be specifically cleaved by ONOO<sup>-</sup> with a ratiometric fluorescence signal enhancement of 94-fold. With the support of ONOO<sup>-</sup> imaging in immune stimulated cells and acute inflammation mice assisted by **Ratio-A**, we exploited to visualize ONOO<sup>-</sup> fluctuations in rheumatoid arthritis (RA) of mice. **Ratio-A** could be applied for effectively imaging of RA and rapidly evaluate the treatment response of RA by methotrexate (MTX). It is envisioned that **Ratio-A** is a promising tool for pathological diagnosing and therapeutic assessment in a wide range of diseases, including RA.

## Introduction

As a diffusion-controlled reaction product, peroxynitrite (ONOO<sup>-</sup>) is formed by fusion of nitric oxide radical (•NO) and superoxide (O<sub>2</sub><sup>•-</sup>).<sup>1-3</sup> Being a strong oxidant and nucleophile, ONOO<sup>-</sup> can damage a wide range of critical molecular components in cells, including proteins, lipids, and DNA, and eventually causing cell death.<sup>4,5</sup> There are research evidences demonstrate that ONOO<sup>-</sup> is the main cause of cytotoxicity, which is previously attributed to the precursors O<sub>2</sub><sup>•-</sup> and •NO.<sup>6,7</sup> Therefore, ONOO<sup>-</sup> has been linked to a growing list of diseases, such as neurological disorders, cancer, rheumatoid arthritis, inflammatory and autoimmune diseases.<sup>8,9</sup> Emerging data have shown that ONOO<sup>-</sup> can be produced by immune cells such as macrophages to kill invading microorganisms to play protective role in immune system.<sup>10</sup> Studies indicate that ONOO<sup>-</sup> also plays crucial roles in the regulation of pivotal signaling pathways by nitrosylation. To deep investigate the pathophysiological roles of ONOO<sup>-</sup>, there is an imperious demand to develop a method to sensitively and unambiguously detect ONOO<sup>-</sup> both *in vitro* and *in vivo*. As ONOO<sup>-</sup> has short half-life (< 10 ms) and exhibits low steady-state concentration (nM range),<sup>11,12</sup> it is still a challenging issue to efficiently detect ONOO<sup>-</sup> *in vitro* and *in vivo*.

Fluorescence imaging, which features sensitivity, selectivity, being noninvasive and real-time spatial imaging capacity, is an attractive tool for ONOO<sup>-</sup> detection.<sup>13-15</sup> During the past several years, numerous fluorescent probes have been constructed for ONOO<sup>-</sup> detection, which enable us to understand the roles of ONOO<sup>-</sup> in specific biological progresses.<sup>16-20</sup> However, most of these probes are intensity-based mode, the application is susceptible by variations from performance of instruments, intracellular microenvironment, local concentrations of the probe and photobleaching. Ratiometric fluorescent probes with

effective internal calibration can avoid these interferences. Therefore, ratiometric fluorescent probes for ONOO<sup>-</sup> detection are urgently required.

Rheumatoid arthritis (RA) is a chronic inflammatory disorder, characterized by hyperplasia of synovium, inflamed joints, bone damage and even disability.<sup>21</sup> RA is an autoimmune disease of unknown etiology, however, studies indicate that oxidative damage induced by reactive oxygen species (ROS) is related to the pathophysiology of RA.<sup>22,23</sup> As a reactive oxidant, ONOO<sup>-</sup> is utilized by phagocytes to kill invading microorganisms, simultaneously inflicts damage on adjacent tissues, and is deemed to be of pathogenic significance in RA progression.<sup>24</sup> However, the exact roles of ONOO<sup>-</sup> in RA are still needed to be further investigated. In addition, the assessment of RA treatment effect in mice with antiarthritic drug, methotrexate (MTX)<sup>25,26</sup> is lacking visual tool. Therefore, it is still desirable to develop ratiometric probes for monitoring ONOO<sup>-</sup> fluctuation in RA progress, for directly reporting oxidative stress during treatment and to get deep insights into the drug therapeutic mechanism.

**Ratio-A** and **Ratio-B** were constructed based on a modified Rhodamine scaffold **QF**,<sup>27,28</sup> which exhibited an emission maximum at 564 nm. Zhang's group have reported a mitochondria targeted probe based on Rhodamine scaffold,<sup>40</sup> the ratiometric probe **Mito-WQPhOH** was successfully applied in living cells to monitor ONOO<sup>-</sup>. The differences of the previous work is that we have changed the conjugating mode by optimizing the sensing moiety. Therefore, the emission wavelength of our probes are extended to the near infrared (≥ 700 nm) region, and the Stokes shift, response time and detection limit of our probes have been considerably improved. It is anticipated that our probes could be employed in living cells, for diagnosis and therapeutic assessment in rheumatoid arthritis model.

## 2. Experiments Section

### 2.1. Synthesis

#### 2.1.1 Synthesis of QF

**QF** was synthesized according to the previous literature.<sup>29</sup> Cyclohexanone (441 mg, 4.5 mmol, 1.5 equivalents) was dropped

<sup>†</sup>The Key Laboratory of Life-Organic Analysis, Key Laboratory of Pharmaceutical Intermediates and Analysis of Natural Medicine, School of Chemistry and Chemical Engineering, Qufu Normal University, Qufu 273165, P.R. China.

\* E-mail: lilizanzan@163.com, jmyou6304@163.com

Electronic Supplementary Information (ESI) available: [details of any supplementary information available should be included here]. See DOI: 10.1039/x0xx00000x

into the ice-cooled concentrated H<sub>2</sub>SO<sub>4</sub> (15 mL) and then stirred for 30 min, 940 mg 2-(4-diethylamino-2-hydroxybenzoyl) benzoic acid (3 mmol) was dissolved into the above solution in portions and then heated to 95 °C for 3 h. The solution was cooled down to room temperature and poured into 100 g of ice. Afterwards, 70 % perchloric acid (5 mL) was dropped to the above solution slowly to obtain red precipitate. The precipitate was filtered off, and then washed with 100 mL cold water. Finally, the precipitate was recrystallized with 5 mL of acetic acid to obtain purple solid (993.17 mg, 83 %). <sup>1</sup>H NMR (500 MHz, CDCl<sub>3</sub>) δ 8.27 (d, *J* = 7.7 Hz, 1H), 7.75 (t, *J* = 7.3 Hz, 1H), 7.66 (t, *J* = 7.6 Hz, 1H), 7.20 (d, *J* = 7.4 Hz, 1H), 7.06 (dd, *J* = 16.5, 9.5 Hz, 2H), 6.85 (s, 1H), 3.61 (d, *J* = 7.0 Hz, 4H), 3.09 (s, 2H), 2.33 – 2.16 (m, 2H), 1.96 (s, 2H), 1.76 (d, *J* = 5.1 Hz, 2H), 1.30 (s, 6H). <sup>13</sup>C NMR (126 MHz, CDCl<sub>3</sub>) δ 170.16, 166.59, 165.31, 159.53, 155.71, 134.30, 133.30, 131.84, 130.36, 130.27, 129.17, 128.43, 121.94, 118.03, 117.48, 95.48, 54.83, 46.23, 29.58, 25.10, 20.89, 20.84. HR-MS: Calcd. **QF**, 376.1907, found: 376.1901.

### 2.1.2 Synthesis of **Ratio-A**

Compound **QF** (951.4 mg, 2 mmol) and 4-Methoxycinnamaldehyde (427.6 mg, 2.4 mmol, 1.2 equivalents) were dissolved in 15 mL ethanol and stirred for 8 h under reflux. The ethanol was removed under reduced pressure, and the obtained solid was purified by silica gel chromatography with DCM / methanol (100 : 1 to 20 : 1, v/v) to obtain green solid (906.88 mg, 87.2%). <sup>1</sup>H NMR (500 MHz, CDCl<sub>3</sub>) δ 8.09 (d, *J* = 6.3 Hz, 1H), 7.65 (d, *J* = 10.7 Hz, 1H), 7.58 (t, *J* = 7.0 Hz, 1H), 7.48 (d, *J* = 8.2 Hz, 3H), 7.17 (d, *J* = 14.9 Hz, 1H), 7.00 (t, *J* = 11.2 Hz, 2H), 6.86 (d, *J* = 8.3 Hz, 2H), 6.80 (d, *J* = 11.1 Hz, 1H), 6.77 (d, *J* = 8.9 Hz, 1H), 6.65 (d, *J* = 8.2 Hz, 1H), 3.80 (s, 3H), 3.50 (d, *J* = 6.2 Hz, 4H), 2.64 (s, 2H), 2.23 (s, 1H), 1.99 (d, *J* = 14.1 Hz, 1H), 1.66 (d, *J* = 24.3 Hz, 2H), 1.23 (dd, *J* = 13.6, 7.0 Hz, 6H). <sup>13</sup>C NMR (126 MHz, CDCl<sub>3</sub>) δ 169.68, 160.58, 156.44, 153.28, 141.51, 135.16, 132.16, 132.01, 129.73, 129.67, 129.52, 129.16, 126.69, 122.08, 114.27, 114.19, 96.23, 55.42, 45.55, 29.67, 25.15, 21.17, 12.63. HR-MS: Calcd. **Ratio-A**, 520.2482, found: 520.2483.

### 2.1.3 Synthesis of **Ratio-B**

Compound **QF** (951.4 mg, 2 mmol) and 4-(dimethylamino) cinnamaldehyde (420.5 mg, 2.4 mmol, 1.2 equivalents) were dissolved in 15 mL ethanol and stirred for 8 h under reflux. The ethanol was removed under reduced pressure and the obtained solid was purified by silica gel chromatography with DCM / methanol (100 : 1 to 15 : 1, v/v) to obtain green solid (891.17 mg, 83.6 %). <sup>1</sup>H NMR (500 MHz, CDCl<sub>3</sub>) δ 8.16 (d, *J* = 7.5 Hz, 1H), 7.63 (d, *J* = 11.4 Hz, 1H), 7.57 (t, *J* = 7.3 Hz, 1H), 7.50 (t, *J* = 7.4 Hz, 1H), 7.44 (d, *J* = 8.3 Hz, 2H), 7.13 (d, *J* = 14.9 Hz, 1H), 7.02 (d, *J* = 7.3 Hz, 1H), 6.99 – 6.93 (m, 1H), 6.79 (d, *J* = 9.1 Hz, 1H), 6.71 (s, 1H), 6.67 (d, *J* = 8.3 Hz, 2H), 6.61 (d, *J* = 9.1 Hz, 1H), 3.49 (d, *J* = 6.9 Hz, 4H), 3.02 (s, 6H), 2.65 (s, 2H), 2.30 (s, 1H), 2.04 (d, *J* = 16.2 Hz, 1H), 1.71 (d, *J* = 34.9 Hz, 2H), 1.24 (s, 6H). <sup>13</sup>C NMR (126 MHz, CDCl<sub>3</sub>) δ 169.08, 158.19, 156.24, 152.83, 151.30, 143.07, 136.11, 132.36, 132.00, 129.66, 129.52, 129.32, 126.51, 124.99, 124.87, 119.84, 118.03, 118.00, 113.46, 113.13, 112.21, 105.01, 96.06, 53.37, 45.28, 40.26, 25.18, 21.16, 12.77. HR-MS: Calcd. **Ratio-B**, 533.2799, found: 533.2792.

### 2.1.4 Preparation of **P1** and **P2**

A mixture of **Ratio-A** (31 mg, 0.05 mmol) and ONOO<sup>-</sup> (2.82 mmol/L, 35 mL) in 10 mL PBS solution was stirred at room

temperature. After completion of the reaction (as monitored by TLC), the mixture was concentrated under reduced pressure and extracted with dichloromethane. The organic layer was dried over Na<sub>2</sub>SO<sub>4</sub> and concentrated under vacuum. And then the products were purified by silica gel chromatography with DCM / methanol (100 : 1 to 30 : 1, and 100 : 1 to 25:1 v/v) to obtain white solid **P2** (1.97 mg, 26.1%) and clay bank solid **P1** (4.38 mg, 22.5%). **P1**: <sup>1</sup>H NMR (400 MHz, CDCl<sub>3</sub>) 7.97 (1 H, t, *J* 6.6), 7.69 (1 H, td, *J* 7.5, 1.1), 7.59 (1 H, dd, *J* 7.5, 0.8), 7.21 (1 H, t, *J* 6.6), 6.52 (1 H, d, *J* 2.6), 6.49 (1 H, d), 6.37 (1 H, dd, *J* 9.0, 2.6), 3.33 (4 H, q, *J* 7.1), 2.63 (2 H, m), 2.27 (1 H, m), 1.97 (2 H, m), 1.78 (1 H, m), 1.14 (6 H, t, *J* 7.1). <sup>13</sup>C NMR (101 MHz, CDCl<sub>3</sub>) 192.29, 169.55, 151.93, 151.42, 149.58, 144.04, 135.04, 129.87, 128.34, 126.80, 125.22, 124.68, 123.43, 109.39, 103.32, 97.73, 84.39, 44.45, 38.18, 22.90, 21.89, 12.47. HR-MS: Calcd. **P1**, 390.1700, found: 390.1700. **P2**: <sup>1</sup>H NMR (400 MHz, DMSO) 12.61 (1 H, s), 7.93–7.87 (2 H, m), 7.04–7.00 (2 H, m), 3.83 (3 H, s). <sup>13</sup>C NMR (101 MHz, DMSO) 167.47, 163.30, 131.80, 123.42, 114.27, 55.89. HR-MS: Calcd. **P2**, 151.0401, found: 151.0406.

### 2.2. Evaluation of **Ratio-A** for ONOO<sup>-</sup> imaging in live cells

RAW264.7 cells were incubated in DMEM medium with 10 % FBS at 37 °C, the humidified CO<sub>2</sub> atmosphere was set as 5 %. The selectivity of **Ratio-A** for exogenous ONOO<sup>-</sup> imaging in living cells was validated by employing ROS and RNS donors. 3-morpholiniosydnonimine hydrochloride (SIN-1) was used for generating ONOO<sup>-</sup>.<sup>30</sup> •NO was generated from 3, 3-bis(aminoethyl)-1-hydroxy-2-oxo-1-triazene (NOC-18), O<sub>2</sub><sup>-</sup> was from menadione sodium bisulfite (MSB), and FeTMPyP was used for consuming ONOO<sup>-</sup>.<sup>18,31</sup> **Ratio-A** were co-incubated with RAW264.7 cells for 30 min, after that the cells were stained with 4, 6-diamidino-2-phenylindole (DAPI, 100 ng/mL, 1 μL) and then washed with phosphate buffered saline (PBS), 50 μM SIN-1, 500 μM NOC-18, 100 μM MSB, 50 μM SIN-1 and 50 μM FeTMPyP were co-incubated for 1 h, respectively. Under the confocal fluorescence microscope, the excitation was set as 488 nm and 594 nm, corresponding emission were set as 520–600 nm (green channel) and 670 nm–750 nm (red channel), blue channel: 430–480 nm (λ<sub>ex</sub>=405 nm).

The evaluation of intracellular retention of **Ratio-A** and the stability of fluorescent product. RAW264.7 cells were stained with **Ratio-A** (10 μM) for 30 min. the control group was treated with PBS solution, and the experimental group were treated with 50 μM SIN-1 for 30 min. The medium was removed and cells were washed with PBS for three times, and then images were acquired at indicated time points.

The assessment of **Ratio-A** to visualize the production of endogenous ONOO<sup>-</sup>. RAW264.7 cells were stimulated with 1 μg/mL lipopolysaccharides (LPS), 100 ng/mL of interferon-gamma (IFN-γ) and 10 nM phorbol 12-myristate 13-acetate (PMA).<sup>32</sup> Aminoguanidine (AG, iNOS inhibitor) and apocynin (NOX inhibitor) were used to conduct enzyme inhibition assay.<sup>33</sup> RAW264.7 cells were divided into four groups. The first group was set as control group; the second group was pre-incubated with LPS and IFN-γ for 15 h, followed by PMA for 1 h; the third group was incubated with 5 mM AG for 4 h before LPS and IFN-γ

for 15 h, and 10 nM PMA for 1 h; the fourth group was pre-treated with 100  $\mu$ M apocynin for 1 h, LPS and IFN- $\gamma$  for 15 h and then 10 nM PMA for 1 h. **Ratio-A** was incubated for 30 min before imaging.

### 2.3. ONOO<sup>-</sup> imaging in acute inflammation model and CIA mice model.

All animal experiments were performed according to the guidelines issued by The Ethical Committee of Qufu Normal University (approval No. QF2018-015L). The evaluation of endogenous ONOO<sup>-</sup> levels in acute inflammation mouse model.<sup>34</sup> Three groups of Kunming mice were employed, the first group mice were treated with saline; the experimental group mice were administered with intraperitoneal (i.p.) injection of 100  $\mu$ L LPS (200  $\mu$ M in saline) to induce peritonitis; the enzyme activity blocking group was treated with 4 mM apocynin followed by 100  $\mu$ L LPS (200  $\mu$ M in saline), 100  $\mu$ L **Ratio-A** (200  $\mu$ M in saline) was injected in the same position 4 h later. *In vivo* images were acquired at 30 min.

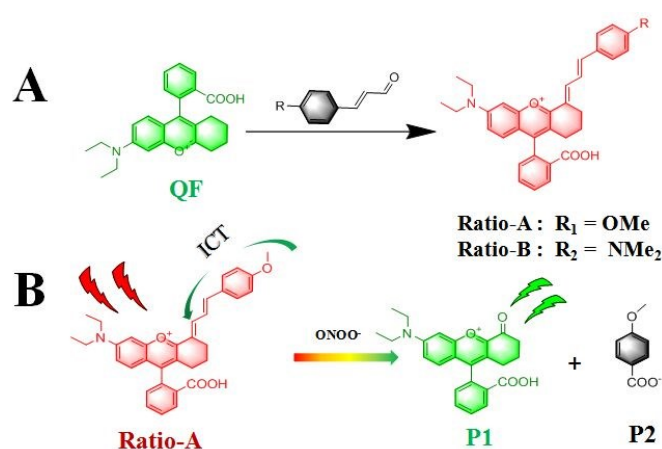
Collagen-induced arthritis (CIA) model was established in male Kunming mice (8-10 weeks) according to the published approach. To establish CIA model, all Kunming mice were randomly divided into four groups. Three groups of mice were injected with 2.0 mg/mL Bovine type II collagen (BCol II) intradermally, which was emulsified in equal volume of complete 2.0 mg/mL of Freund's Adjuvant (CFA) in tail. A booster immunization was operated at 21 days after the primary immunization, which was treated with BCol II, equally emulsified in incomplete Freund's Adjuvant (IFA).<sup>35</sup> To evaluate the therapeutic efficacies of glutathione (GSH) and MTX, one group of the CIA mice were administrated with saline, another two groups of CIA mice were administrated with GSH (200 mg/kg body weight) and MTX (5.0 mg/kg body weight), respectively. All mice were intravenously administrated every 3 days, and all treatments were repeated six times for each group. Fluorescence imaging was performed at 3 days after the last injection.

## 3. Results and discussions

### 3.1. Design and Synthesis of ratiometric fluorescent probes

Rhodamine dyes has excellent optical characteristics, such as good photo-stability and high fluorescence quantum yields.<sup>36</sup> However, the Stokes shift of Rhodamine derivatives is generally less than 50 nm, which results in background interference in fluorescence imaging. We selected the structural improved Rhodamine fluorophore, **QF** for skeleton and obtained **Ratio-A** and **Ratio-B** (Scheme 1) after condensing with cinnamaldehydes with **QF**. The Stokes shifts of **Ratio-A** and **Ratio-B** were more than 100 nm. Furthermore, the probes can avoid interference factors by showing optical changes at two emission bands.<sup>37,38</sup> The detection mechanism towards ONOO<sup>-</sup> is anticipated that butadienyl bridge is oxidized into a carbonyl fluorophore, which is confirmed by high resolution mass spectrum.<sup>39,40</sup> The mass signal ( $m/z$ ) at 390.1701 indicated the carbonyl fluorophore **P1** (calculated value: 390.1700) was formed, and the mass signal ( $m/z$ ) at 151.0406 represented the carboxylic phenyl compound

**P2** in **Ratio-A** (calculated value: 151.0401) (Figure S14). Zhang's group has reported the formation of compound **P1** and confirmed the exact mass.<sup>40</sup> And then we isolated the products after reaction with ONOO<sup>-</sup>, **P1** and **P2** were purified and characterized by <sup>1</sup>HNMR and <sup>13</sup>CNMR to further confirm the proposed sensing mechanism. The corresponding products of **Ratio-B** were also studied and confirmed by HR-MS (Figure S15). HPLC analysis was further used to verify the response mechanism during detection process of **Ratio-A** towards ONOO<sup>-</sup>. As shown in Figure S16, the peaks at 8.07 min and 10.13 min were belonged to the carbonyl fluorophore and carboxylic phenyl compound, and the two peaks were appeared after addition of ONOO<sup>-</sup>, while the peak at 4.82 min (**Ratio-A**) was diminished. The results were consistent with the HR-MS data, which was suggested that the products of **Ratio-A** were generated after the reaction with ONOO<sup>-</sup>.



**Scheme 1.** Structures and the proposed mechanism toward ONOO<sup>-</sup>. (A) The synthesis of **Ratio-A** and **Ratio-B**; (B) The proposed mechanism of **Ratio-A** toward ONOO<sup>-</sup>.

### 3.2. Spectroscopic properties of Ratio-A and Ratio-B

The spectroscopic properties of **Ratio-A** (10  $\mu$ M) and **Ratio-B** (10  $\mu$ M) were evaluated in physiological condition (20 mM PBS, pH 7.4, 0.1% DMSO). The UV-vis absorption responses of **Ratio-A** and **Ratio-B** were investigated. As shown in Figure 1A, the free probe **Ratio-A** possessed a protruding absorption peak at 600 nm and a weak peak at 414 nm. After the addition of ONOO<sup>-</sup> with the concentration of 0-10  $\mu$ M, the absorption peak at 600 nm was reduced and the the absorption peak at 414 nm was enhanced. Meanwhile, the solution colour was changed from blue to yellow (Figure S21). We then tested the fluorescence response of **Ratio-A** to different concentrations of ONOO<sup>-</sup>, and the corresponding fluorescence emission peak at 564 nm was enhanced gradually as well as the fluorescence emission at 700 nm was decreased (Figure 1B and 1C). The fluorescence changes can be ascribed to the disruption of ICT process induced by a specific ONOO<sup>-</sup>-triggered butadienyl bridge cleavage. There was a linear ( $R^2 = 0.993$ ) relationship between logarithm of the fluorescence ratio ( $F_{564 \text{ nm}}/F_{700 \text{ nm}}$ ) and ONOO<sup>-</sup> concentration (0-10  $\mu$ M) (Figure 1D). The detection limit was calculated as 28.06 nM based on  $3\sigma/k$ . Similarly, the absorption peaks of **Ratio-B** were 680 nm and 414 nm (Figure S2A). The solution colour was changed from glaucous to yellow (Figure S21). Upon addition of

ONOO<sup>-</sup>, corresponding emission peak at 808 nm was gradually diminished, and the emission peak at 564 nm increased gradually (Figure. S2B, 2C). The linear ( $R^2 = 0.967$ ) relationship between logarithm of the ratio ( $F_{564\text{ nm}}/F_{808\text{ nm}}$ ) and ONOO<sup>-</sup> (0–10  $\mu\text{M}$ ) was shown in Figure S2D. The detection limit was calculated as 652.03 nM. The absolute quantum yields of **Ratio-A** ( $\Phi = 4.67\%$ ) at 700 nm were much higher than **Ratio-B** ( $\Phi = 0.068\%$ ). The fluorescence lifetimes of **Ratio-A** were 4.3226 ns (dominant, 85.32%) and 100 ns (minor, 14.68%) (Figure S19), whereas the lifetimes of **Ratio-B** were 0.6965 ns (dominant, 6.15%) and 4.4136 ns (minor, 93.85%) on account of the various installed groups (Figure S20).

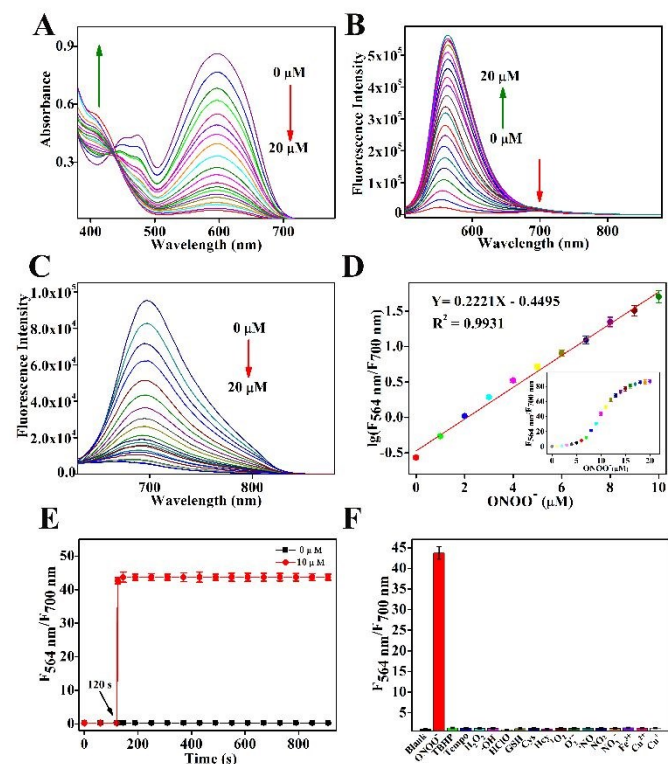


**Figure 1.** Spectral properties of **Ratio-A** (10  $\mu\text{M}$ ) in PBS solution (pH=7.4, 20 mM, with 0.1% DMSO). Data were recorded 10 min after the addition of ONOO<sup>-</sup>. (A) UV absorption spectra of **Ratio-A** in the presence of ONOO<sup>-</sup> (0–10  $\mu\text{M}$ ). (B) Emission spectra of **Ratio-A** at 564 nm with concentrations of ONOO<sup>-</sup> (0–10  $\mu\text{M}$ ). ( $\lambda_{\text{ex}} = 480\text{ nm}$ ). (C) Emission spectra of **Ratio-A** at 700 nm ( $\lambda_{\text{ex}} = 600\text{ nm}$ ). (D) The linear relationship between  $\log(F_{564\text{ nm}}/F_{700\text{ nm}})$  and ONOO<sup>-</sup>. Insert: ratio values with different concentrations of ONOO<sup>-</sup>. (E) Time dependent fluorescence ratios ( $F_{564\text{ nm}}/F_{700\text{ nm}}$ ) of **Ratio-A** toward ONOO<sup>-</sup> (0  $\mu\text{M}$ , 10  $\mu\text{M}$ ) during 0–900 s, probe was added at 120 s. (F) Ratiometric fluorescence responses ( $F_{564\text{ nm}}/F_{700\text{ nm}}$ ) of **Ratio-A** toward ONOO<sup>-</sup> (10.0  $\mu\text{M}$ ) and other ROS/RNS/RSS (20 equivalents), metal ions (20 equivalents). The error bars represent  $\pm$  S.D. ( $n=3$ ).

### 3.3. Selectivity studies of Ratio-A and Ratio-B

To further evaluate the selectivity of **Ratio-A** and **Ratio-B** toward ONOO<sup>-</sup>, the fluorescence spectra were recorded in the absence and presence of various biologically relevant species. The results of **Ratio-A** were illustrated in Figure 1F. **Ratio-A** exhibited 94-fold ratiometric fluorescence enhancement towards ONOO<sup>-</sup> compared with the blank group, while other species caused negligible ratiometric signal changes even in the presence of 20 equivalents. The results of **Ratio-B** were shown in Figure S2F, the  $\bullet\text{OH}$  radical caused a 12-fold ratiometric enhancement.  $\bullet\text{NO}$  radicals, TBHP,  $^1\text{O}_2$  and  $\text{H}_2\text{O}_2$  can induce

distinct changes in the ratio values of **Ratio-B**. The pH effects on the **Ratio-A** and its sensing reaction in different pH buffer were also investigated. The results showed that **Ratio-A** was stable in the range of pH 4.5–8.5, and the recognition of ONOO<sup>-</sup> was not affected in physiological condition (Figure S3). Furthermore, the fluorescence ratio values of **Ratio-A** were investigated in varied polarity of solvents (Figure. S4). The results showed that the ratio values were essentially constant, which indicated that **Ratio-A** was insensitive to different polarity.

Characteristics of high stability and fast recognition are necessary to the desirable probes. The reaction kinetics of **Ratio-A** on ONOO<sup>-</sup> was studied. As shown in Figure 1E, the fluorescence ratio values of **Ratio-A** reached maximum in 10 s and stayed constant for 15 min after the addition of ONOO<sup>-</sup>. The reaction kinetics of **Ratio-B** on ONOO<sup>-</sup> was shown in Figure S2E, **Ratio-B** also exhibits fast recognition and stability.

### 3.4. Exogenous and endogenous ONOO<sup>-</sup> imaging in RAW 264.7 cells

After investigating the chemical performance of **Ratio-A**, we next evaluated the capability of **Ratio-A** in RAW264.7 cells for detection of exogenous and endogenous ONOO<sup>-</sup>. Cytotoxicity was assessed by Cells Counting Kit-8 (CCK-8) assay. As illustrated in Figure S17, **Ratio-A** showed low cytotoxicity even in the concentration of 100  $\mu\text{M}$ , thus the probe was suitable for living cell imaging. RAW264.7 cells were selected as the cell model, ROS and RNS donors were employed to evaluate the selectivity of **Ratio-A** in RAW264.7 cells. Fluorescence imaging was displayed in Figure 2A, and the pseudo-color ratiometric images were presented to illustrate the ratios of green channel versus red channel. The fluorescence signal in the control group showed weak fluorescence in green channel and strong fluorescence in red channel, which were consistent with the fluorescence spectra of free probe **Ratio-A** (Figure 2B, 2C). As shown in Figure 2A, the blue channel indicated that the probes did not enter into the nucleus of the cells. Obvious enhancement of the intracellular fluorescence ratios were observed after treating with SIN-1, rather than treated with NOC-18 and MSB. The increased fluorescence ratio in SIN-1-treated cells were attenuated after addition of ONOO<sup>-</sup> scavenger FeTMPyP, which was suggested that **Ratio-A** exhibited significant stability to other biological species and showed high selectivity toward ONOO<sup>-</sup> in living cells. The ratiometric fluorescence variations in flow cytometry analysis further verified the selective ONOO<sup>-</sup> detecting capacity of **Ratio-A** (Figure 2A and 2B).

The intracellular retention of **Ratio-A** was evaluated by means of fluorescence ratio values ( $F_{\text{green}}/F_{\text{red}}$ ) (Figure S18A), and the ratio values of **Ratio-A** in RAW264.7 cells stayed constant over two hours (Figure S18C). The fluorescence ratio values were further confirmed by flow cytometry analysis (Figure S18B). The results suggested that **Ratio-A** and the reaction products can retain in cells due to the negatively charged carboxylates.<sup>41</sup>

**Ratio-A** was used to explore the imaging of endogenous ONOO<sup>-</sup> in RAW264.7 cells after stimulation. As shown in Figure 3A and

3C, the ratio of green channel versus red channel was enhanced distinctly after stimulation with LPS/IFN- $\gamma$ /PMA.

View Article Online  
DOI: 10.1039/D0TB01970D

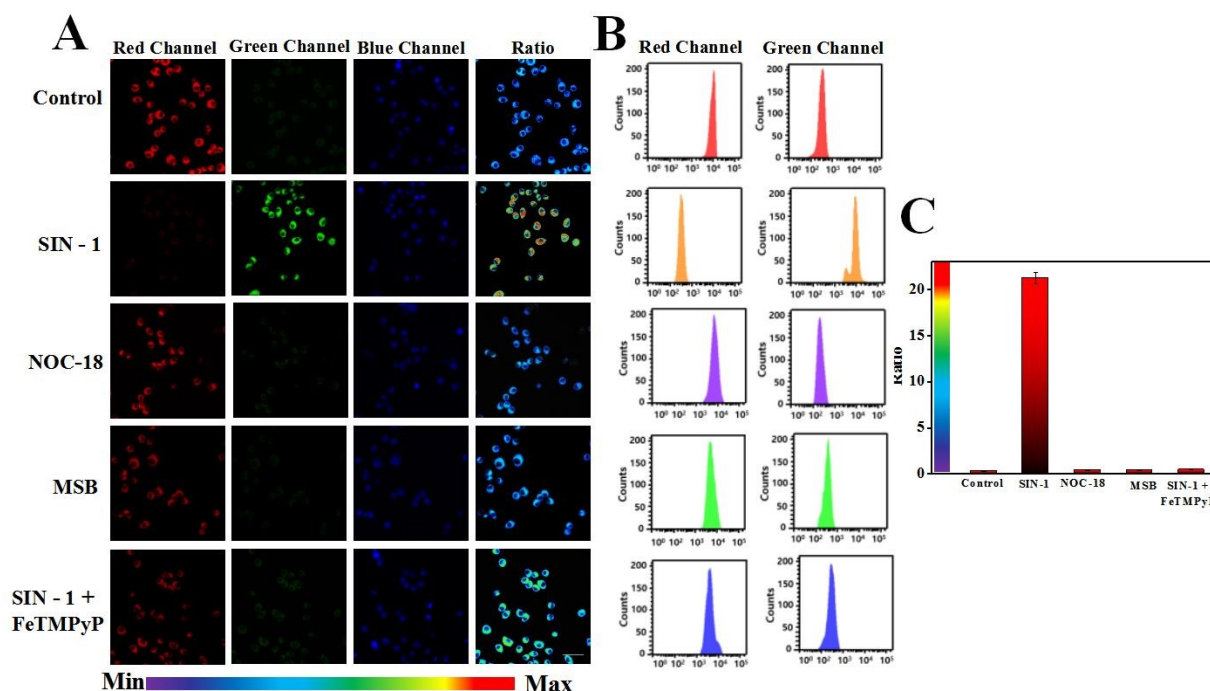


**Figure 2.** Validation the selectivity of **Ratio-A** (10  $\mu$ M) with ROS/RNS donors by confocal imaging and flow cytometry analysis in RAW264.7 cells. (A). Cells were loaded with **Ratio-A** and then treated with SIN-1 (50  $\mu$ M), NOC-18 (500  $\mu$ M), and MSB (100  $\mu$ M) respectively to produce ONOO $^-$ ,  $\bullet$ NO, O $_2^{\bullet-}$ . FeTMPyP (50  $\mu$ M) was used to decompose ONOO $^-$ . (B). Flow cytometry analysis of the cells in corresponding group of (A). (C) The fluorescence ratio values ( $F_{green}/F_{red}$ ) of (A). Scale bar represents 20  $\mu$ m. The experiments were repeated three times and the data were shown as mean ( $\pm$  S.D.).

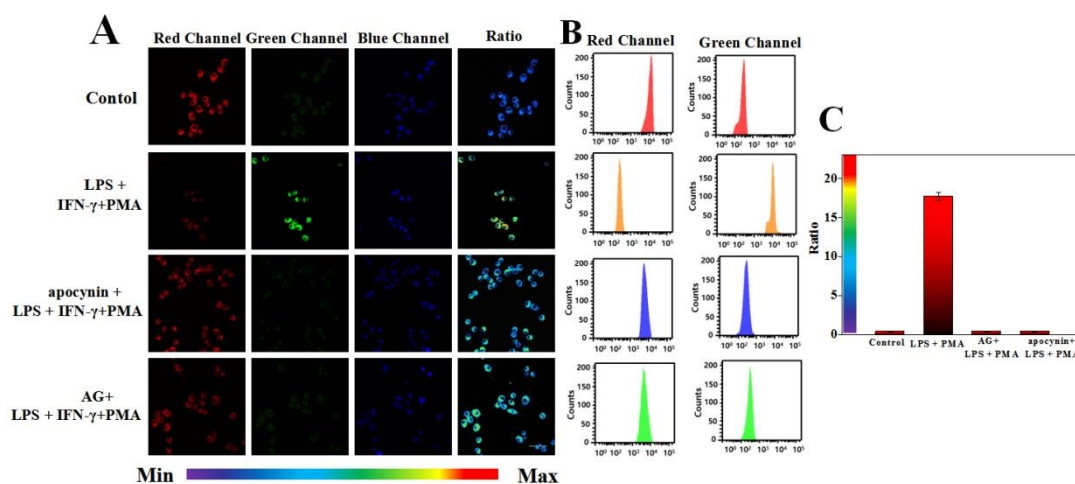


**Figure 3.** Confocal imaging of endogenous ONOO $^-$  with **Ratio-A** (10  $\mu$ M) in stimulated RAW264.7 cells. (A) Cells were treated with LPS (1  $\mu$ g/ml), and IFN- $\gamma$  (100 ng/ml), followed by PMA (10 nM), and then stained with **Ratio-A** before imaging. AG (5 mM) and apocynin (100  $\mu$ M) were added at the onset of immune stimulation to reduce the level of  $\bullet$ NO or O $_2^{\bullet-}$ , respectively. (B). Flow cytometry analysis of the cells in corresponding group of (A). (C) The fluorescence ratio values ( $F_{green}/F_{red}$ ) of (A). Scale bar represents 20  $\mu$ m. The experiments were repeated three times, the error bars represent  $\pm$  S.D. (n=3)

After the cells were incubated with NOX inhibitor, apocynin (100  $\mu$ M) and iNOS inhibitor aminoguanidine (AG, 5 mM), the green fluorescence of **Ratio-A** was effectively suppressed. These results demonstrated that the fluorescence changes of **Ratio-A** in murine RAW264.7 cells can be ascribed to the ONOO<sup>-</sup> generation. The fluorescence ratios detected by flow cytometry analysis were consistent with the cell imaging using confocal microscope (Figure 3B). Collectively, it was suggested that **Ratio-A** was suitable for ONOO<sup>-</sup> selectively imaging in living cells.

### 3.5. ONOO<sup>-</sup>-related inflammatory response in mice

Studies demonstrated that excessively endogenous ONOO<sup>-</sup> production is a pivotal mediator in inflammation.<sup>8</sup> Based on the ONOO<sup>-</sup> imaging capacity of **Ratio-A**, we further applied **Ratio-A** for visualizing endogenous ONOO<sup>-</sup> in acute inflammation mice model. As displayed in Figure 4, the fluorescence intensity from experimental group was remarkably increased in green channel, while the fluorescence intensity in red channel was obviously decreased compared with control group. As was shown in Figure 4b, the ratio was increased by 30 times at 30 min compared with control group. While the ratio of apocynin treated group stayed unchanged (Figure 4c), which indicated that the generation of ONOO<sup>-</sup> was blocked after treating with apocynin. The results revealed that ONOO<sup>-</sup> was transported and accumulated in the inflamed sites. Thus, **Ratio-A** could be employed to visualize the generation of endogenous ONOO<sup>-</sup> in acute inflammation mice model.

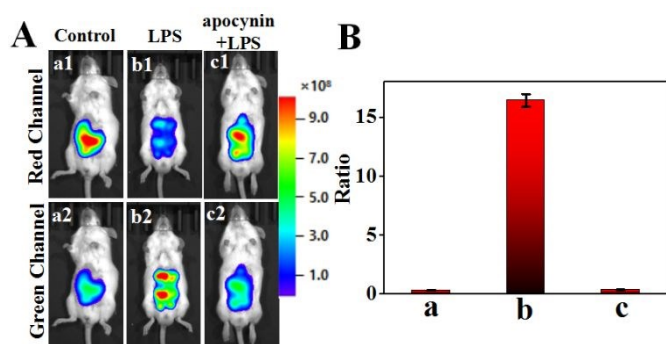


**Figure 4.** Imaging of endogenous ONOO<sup>-</sup> in acute inflammatory mice. Red channel: 670–750 nm, green channel: 520–600 nm. (A). (a). The control group were treated with saline, and **Ratio-A** was injected into the inflamed site. (b). Mice were stimulated with LPS for 4 h, and then the **Ratio-A** was injected. (c). Mice were treated with apocynin, and then stimulated with LPS. Images were acquired at 30 min. (B). The ratiometric fluorescence intensity ( $F_{\text{green}}/F_{\text{red}}$ ) of (A). The experiments were repeated three times and the data were shown as mean ( $\pm$  S.D.).

### 3.6. Imaging of RA in Mice

Autoimmune arthritis models have become valuable research models for studying pathogenic mechanisms and developing new therapies.<sup>42</sup> CIA model was widely used for studying the process of rheumatoid arthritis (RA).<sup>43</sup> There was an increasing evidence to indicate that ROS play a vital role in the RA pathogenesis.<sup>23,44</sup> The activated phagocytic cells, including neutrophils and macrophages, can produce highly toxic ROS in the process of oxidative burst to kill the invading pathogens. ONOO<sup>-</sup> was then formed by the fusion of •NO and O<sub>2</sub><sup>•-</sup>, which

was thought to be of pathogenic significance in RA.<sup>45</sup> the possibility of **Ratio-A** for assessing the treatment of RA model in mice. As shown in Figure 5A and 5B, CIA mice treated with saline showed a significant decrease in red fluorescence channel and an obvious enhancement in green fluorescence channel after injected with **Ratio-A**, while the fluorescence ratio signal ( $F_{\text{green}}/F_{\text{red}}$ ) at the ankle joints were reduced after treating with GSH and MTX. The above results indicated that **Ratio-A** was capable of monitoring ONOO<sup>-</sup> in CIA mice, and GSH as well as MTX can restrain the levels of ONOO<sup>-</sup>.<sup>45,46</sup> Subsequently, the mice were sacrificed, and the knee joints were collected. Histological analysis of knee joints was performed by hematoxylin and eosin (H&E) staining. As shown in Figure 5C, the articular cartilages were eroded and became roughly and thinly in the RA mice model, the blue stained inflammatory cells invaded into the hyperplastic synovium. It was suggested that the degree of ankle tissue injury treated with MTX had been alleviated. The above experiments results demonstrated that **Ratio-A** can be utilized for evaluating the variations of ONOO<sup>-</sup> levels in CIA mice model. As an effective fluorescent probe, **Ratio-A** can be used for RA diagnosis by monitoring ONOO<sup>-</sup> fluctuations.

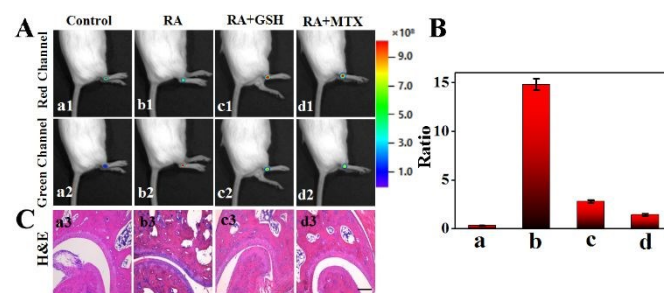


**Figure 5.** Visualization of ONOO<sup>-</sup>-mediated inflammatory response in the RA model. (A). Fluorescence images of mice in group a–d. a: control group; b: RA mice; c: GSH treated RA mice; d: MTX treated RA mice. The mice were injected with **Ratio-A** (50  $\mu$ M) before imaging. (B). Fluorescence ratio values ( $F_{\text{green}}/F_{\text{red}}$ ) in (A). (C). The corresponding H&E staining of ankle joints tissues. Scale bar: 200  $\mu$ m.

## 4 Conclusion

In summary, two ratiometric fluorescent probes, **Ratio-A** and **Ratio-B** were synthesized for ONOO<sup>-</sup> detection. **Ratio-A** exhibited excellent selectivity towards ONOO<sup>-</sup> compared to **Ratio-B** under physiological conditions. The responding mechanism of **Ratio-A** towards ONOO<sup>-</sup> was confirmed by HR-MS and HPLC analysis, and <sup>1</sup>HNMR, <sup>13</sup>CNMR. **Ratio-A** exhibited high sensitivity for ONOO<sup>-</sup> with a 94-fold ratio enhancement and excellent selectivity over various biological species, the detection limit was as low as 28.06 nM. Moreover, the large Stokes shift (> 100 nm) and low cytotoxicity endowed **Ratio-A** with the capacity of real time monitoring intracellular ONOO<sup>-</sup> fluctuations in immune stimulated RAW264.7 cells and acute inflammatory model. Importantly, the ONOO<sup>-</sup> related inflammatory response in RA and the response of RA treatment were successfully demonstrated with the assist of **Ratio-A**. It is envisioned that **Ratio-A** can contribute to future clinical researches on RA diagnosis, treatment response monitoring,

and the etiology studies of ONOO<sup>-</sup>-mediated inflammatory disorders, which can further illuminate the ONOO<sup>-</sup> biology.

### Conflicts of interest

There are no conflicts to declare.

### Acknowledgements

This work was financially supported by the National Natural Science Foundation of China (No. 21976105).

### Notes and references

- J. S. Beckman, T. W. Beckman, J. Chen, P. A. Marshall and B. A. Freeman, *Proc. Natl. Acad. Sci. USA.*, 1990, **87**, 1620–1624.
- R. E. Huie and S. Padmaja, *Free. Radic. Res. Commun.*, 1993, **18**, 195–199.
- G. Ferrer-Sueta and R. Radi, *ACS. Chem. Biol.*, 2009, **4**, 161–177.
- V. M. Darley-usmar, N. Hogg, V. J. O'Leary, M. T. Wilson and S. Moncada, *Free. Radic. Res. Commun.*, 1992, **17**, 9–20.
- L. Virág, É. Szabó, P. Gergely and C. Szabó, *Toxicol. Lett.*, 2003, **140-141**, 113–124.
- J. S. Beckman, *Nature*, 1990, **345**, 27–28.
- W. H. Koppenol, J. J. Moreno, W. A. Pryor, H. Ischiropoulos and J. S. Beckman, *Chemical Research in Toxicology*, 1992, **5**, 834–842.
- P. Pacher, J. S. Beckman and L. Liaudet, *Chem. Res. Toxicol.*, 2007, **87**, 315–424.
- C. Szabó, H. Ischiropoulos and R. Radi, *Nat. Rev. Drug. Discov.*, 2007, **6**, 662–680.
- V. B. Koman, N. R. von Moos, C. Santschi, V. I. Slaveykova and O. J. F. Martin, *Nanotoxicology*, 2016, **10**, 1041–1050.
- C. Ducrocq, B. Blanchard, B. Pignatelli and H. Ohshima, *Cell. Mole. Life. Sci.*, 1999, **55**, 1068–1077.
- D. Yang, H. L. Wang, Z. N. Sun, N. W. Chung and J. G. Shen, *J. Am. Chem. Soc.*, 2006, **128**, 6004–6005.
- M. H. Lee, A. Sharma, M. J. Chang, J. Lee, S. Son, J. L. Sessler, C. Kang and J. S. Kim, *Chem. Soc. Rev.*, 2018, **47**, 28–52.
- S. Singha, Y. W. Jun, S. Sarkar and K. H. Ahn, *Accounts. Chem. Res.*, 2019, **52**, 2571–2581.
- L. Wu, A. C. Sedgwick, X. Sun, S. D. Bull, X.-P. He and T. D. James, *Accounts. Chem. Res.*, 2019, **52**, 2582–2597.
- Z. j. Chen, W. Ren, Q. E. Wright and H. w. Ai, *J. Am. Chem. Soc.*, 2013, **135**, 14940–14943.
- Z. Song, D. Mao, S. H. P. Sung, R. T. K. Kwok, J. W. Y. Lam, D. Kong, D. Ding and B. Z. Tang, *Adv. Mater.*, 2016, **28**, 7249–7256.
- T. Peng, X. Chen, L. Gao, T. Zhang, W. Wang, J. Shen and D. Yang, *Chem. Sci.*, 2016, **7**, 5407–5413.
- J. Zhang, X. Zhen, J. Zeng and K. Pu, *Anal. Chem.*, 2018, **90**, 9301–9307.
- D. Li, S. Wang, Z. Lei, C. Sun, A. M. El-Toni, M. S. Alhoshan, Y. Fan and F. Zhang, *Anal. Chem.*, 2019, **91**, 4771–4779.
- C. Vingsbo-Lundberg, N. Nordquist, P. Olofsson, M. Sundvall, T. Saxne, U. Pettersson and R. Holmdahl, *Nat. Genet.*, 1998, **20**, 401–404.
- C. A. Hitchon and H. S. El-Gabalawy, *Arthritis. Res. Ther.*, 2004, **6**, 265.
- H. M. Khojah, S. Ahmed, M. S. Abdel-Rahman and A. B. Hamza, *Free. Radical Bio. Med.*, 2016, **97**, 285–291.
- F. C. Fang, *Nat. Rev. Microbiol.*, 2004, **2**, 820–832.
- S. Majumdar, M. E. Anderson, C. R. Xu, T. V. Yakovleva, L. C. Gu, T. R. Malefyt and T. J. Siahaan, *J. Pharm. Sci.*, 2012, **101**, 3275–3291.
- S. Rexhepi, M. Rexhepi, B. Rexhepi, V. Sahatçiu-Meka and V. Mahmutaj, *Arthritis. Res. Ther.*, 2012, **14**, 60.
- Y. Q. Sun, J. Liu, X. Lv, Y. Liu, Y. Zhao and W. Guo, *Angew. Chem. Int. Ed.*, 2012, **51**, 7634–7636.
- L. Wang, W. Du, Z. Hu, K. Uvdal, L. Li and W. Huang, *Angew. Chem. Int. Ed.*, 2019, **58**, 14026–14043.
- W. L. Jiang, Y. Li, W. X. Wang, Y. T. Zhao, J. Fei and C. Y. Li, *Chem. Commun.*, 2019, **55**, 14307–14310.
- S. R. Thomas, M. J. Davies and R. Stocker, *Chem. Res. Toxicol.*, 1998, **11**, 484–494.
- S. Rausaria, A. Kamadulski, N. P. Rath, L. Bryant, Z. Chen, D. Salvemini and W. L. Neumann, *J. Am. Chem. Soc.*, 2011, **133**, 4200–4203.
- H. Yamada, T. Arai, N. Endo, K. Yamashita, K. Fukuda, M. Sasada and T. Uchiyama, *Life. Sci.*, 2006, **78**, 926–933.
- Y. Y. Qin, M. Li, X. Feng, J. Wang, L. Cao, X. K. Shen, J. Chen, M. Sun, R. Sheng, F. Han and Z.-H. Qin, *Free. Radica.l Bio. Med.*, 2017, **104**, 333–345.
- S. Wirtz, V. Popp, M. Kindermann, K. Gerlach, B. Weigmann, S. Fichtner-Feigl and M. F. Neurath, *Nat. Protoc.*, 2017, **12**, 1295–1309.
- D. D. Brand, K. A. Latham and E. F. Rosloniec, *Nat. Protoc.*, 2007, **2**, 1269–1275.
- M. Beija, C. A. M. Afonso and J. M. G. Martinho, *Chem. Soc. Rev.*, 2009, **38**, 2410–2433.
- M. Y. Wu, Y. Wang, Y. H. Liu and X. Q. Yu, *J. Mater. Chem. B*, 2018, **6**, 4232–4238.
- Y. Liu, J. Nie, J. Niu, W. S. Wang and W. Y. Lin, *J. Mater. Chem. B*, 2018, **6**, 1973–1983.
- Z. Li, S. H. Yan, C. Chen, Z. R. Geng, J. Y. Chang, C. X. Chen, B. H. Huang and Z. L. Wang, *Biosen. Bioelectron.*, 2017, **90**, 75–82.
- W. Shu, Y. L. Wu, T. J. Shen, J. Cui, H. Kang, J. Jing, X. L. Zhang, *Dyes and Pigments*, 2019, **170**, 107609–107613.
- J. Wang, L. Zhang, F. Peng, X. Shi and D. T. Leong, *Chem. Mater.*, 2018, **30**, 3759–3767.
- P. S. C. Leung, S. A. Shu, T. P. Kenny, P. Y. Wu and M. H. Tao, *Autoimmun. Rev.*, 2010, **9**, 400–405.
- R. Holmdahl, R. Bockermann, J. Bäcklund and H. Yamada, *Ageing. Res. Rev.*, 2002, **1**, 135–147.
- Z. Chen, Z. Liu, Z. Li, E. Ju, N. Gao, L. Zhou, J. Ren and X. Qu, *Biomaterials*, 2015, **39**, 15–22.
- K. Shiozawa, T. Yamane, M. Murata, R. Yoshihara, K. Tsumiyama, S. Imura and S. Shiozawa, *Arthritis. Res. Ther.*, 2016, **18**, 55.
- K. Srisook, C. Kim and Y. N. Cha, *Method. Enzymol.*, 2005, **396**, 414–424.

Endogenous  $\text{ONOO}^-$  generation in rheumatoid arthritis mice was visualized and confirmed assisted by ratiometric fluorescent probe **Ratio-A**

View Article Online  
DOI: 10.1039/D0TB01970D

